SIMPLISTIC ONE POT SYNTHESIS OF ZnO VIA CHELATING WITH CARBOXYLIC ACIDS

K. K. TAHA[a,b,*] , A. MODWI[a], L. KHEZAMI[a,c], M.HEIKAL[a,c]
[a]*Chemistry Department, College of Science, Al Imam Mohammad Ibn Saud Islamic University (IMSIU), P.O Box 90950, Riyadh 11623, Saudi Arabia*
[b]*Department of Chem. & Ind. Chem., College of Appl. & Ind. Sciences, University of Bahri, Khartoum, Sudan*
[c]*Chemistry Department, Faculty of Science, Benha University, Benha, Egypt*

This work highlights a simplistic route for synthesizing zinc oxide nanoparticles via a direct chelating reaction achieved by adding zinc nitrate to dicarboxylic acids namely malonic, succinic and tartaric followed by slow evaporation to form the subsequent complexes. The resulting complexes were thermally treated at $450^{o}C$ for 2h to acquire the ZnO nanoparticles. The Fourier Transformation Infrared (FT-IR) vibrations indicated the bonding of zinc to the carboxylic oxygen as a clue for complex and produced zinc oxide nanoparticles formation. The X-ray diffraction (XRD) data and William Hall method models authenticated the nanosized dimensions (40 – 50 nm) of the acquired nanostructures. In addition, visual evidence was provided by the scanning electron microscopy (SEM) micrographs for the nanoparticles formation. The photoluminescence investigation demonstrated blue and green emissions occurred at 495 and 520 nm respectively. We believe that the preparation method adopted in this work is safe as no toxic chemicals or solvents were used.

1. Introduction

Zinc oxide is an n-type semiconductor material having a wide band gap with a large excitonic binding energy and distinctive photoluminescence (PL) features[1]. It is having a direct band gap semiconductor (E_g= 3.37eV) and possesses a hexagonal wurtzite crystalline structure [2].In addition to its UV excitonic emission peak, ZnO generally shows visible luminescence at a range of emission wavelengths due to the existence of intrinsic or extrinsic defects. In the nanoscale, it acquires fascinating electronics and optical attributes that deem it functional in fabrication of photonics, electronics, and sensor devices. Moreover, ZnO nanostructures have possible utility in optoelectronic gadgets such as solar cells, organic light emitting diodes (OLED) and liquid crystal displays (LCD) by virtue of its large 60 meV exciton binding energy [3, 4].

So far, various techniques including pulse laser deposition, sol gel, spray pyrolysis, mechanical grinding and simple combustion methods for the fabrication of ZnO nanoparticles are reported in the literature [5, 6]. Yet, most of the described procedures are either time consuming or use expensive chemicals in comparison with simple precipitation method. Studies about the use of oxalic acids for preparing Fe_3O_4-NPs [7], $Ni_{1-x}Zn_xO$ nanoparticles and $Ni_{1-x}Zn_xO/ZnO$ nanocomposites[8],indium-based oxides [9],$Ni_{0.9}Zn_{0.1}O/ZnO$ [10] and ZnO [11]were reported.

In the following context, we describe a facile route for the synthesis of ZnO nanoparticles. In a one-pot experiment Zn^{2+} were reacted with dicarboxylic acids to provide the corresponding complexes after a mild evaporation process. The formation of the target ZnO nanoparticles was achieved by calcinations of the coordination compounds at $450^{o}C$. The development of the nanoparticles was confirmed by FTIR, XRD, TEM, BET nitrogen adsorption and PL techniques.

_____
*Corresponding author: kamaltha60@gmail.com

2. Experimental

2.1 Synthesis of ZnO nanoparticles

The intended nanoparticles precursors were prepared by a simple chelating reaction of zinc ions with dicarboxylic acids i.e. succinic, malonic and tartaric acids. Here 0.10 M aqueous solution of each of the acids was added dropwise to 0.10 M solution of $Zn(NO_3)_2.6H_2O$ followed by gentle evaporation at low temperature (70°C). White color complexes of the respective acids (succinate, malonate and tartarate) with Zn^{2+} were left after the water evaporation. The resulting products were calcined at 450°C for 2 h to obtain the ZnO nanoparticles (Scheme 1).
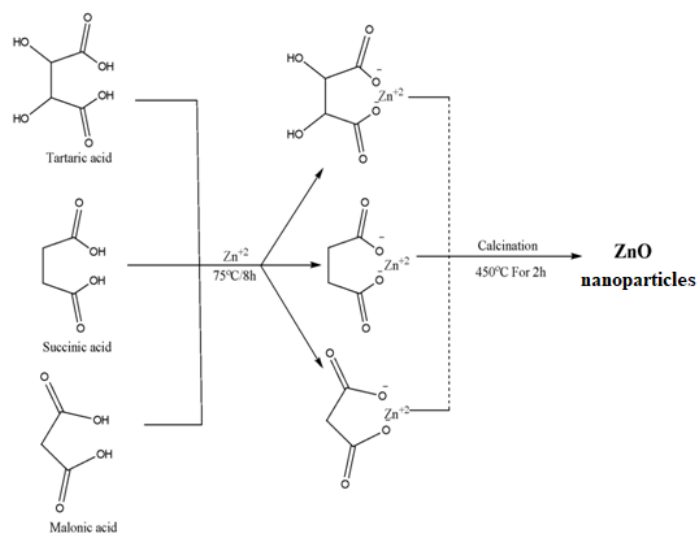
Scheme1. Carboxylic acids chelating with Zn^{2+} and nanoparticles formation

2.2. Characterization techniques

A number of characterization techniques were employed to examine the structure, morphology, chemical bonding and optical properties of the product. The crystal structure of the synthesized nanomaterials was investigated by powder X-ray diffraction (XRD) at room temperature, via D8 Advance diffractometer (Bruker, Germany) with Cu-Kα radiation (λ = 0.15406 nm) at an accelerating voltage of 40 kV and 30 mA emission current. A scanning electron microscope (SEM) (Phenom XL, Netherland) was used to record the morphology of the nanoparticles. The stretching modes of vibration bands of the prepared samples were probed by Fourier transform infrared spectroscopy (Model: Nicolet 6700) in the range 4000 - 400 cm^{-1} with a resolution of 4 cm^{-1}.The thermal stability of the obtained salts was tested by thermal gravimetric analysis TGA (Model: Mettler Toledo) under 0.02 to 250 K/min heating pace from ambient temperature till 1000°C in 150 µL crucible. The fluorescence measurements were carried out in Agilent Cary Eclipse fluorescence spectrophotometer (Agilent technologies, USA) with a Xe flash lamp. The excitation wavelength used was 325nm and the emission spectra were collected.

3. Results and discussion

3.1. Infrared spectra and Zn coordination to carboxylic acids elucidation

FTIR is an appropriate method to study the formation of zinc malonate, succinate and tartrate (Fig. 1). The1750–1700 and 1300–1200 cm^{-1} bands are distinguishing feature of carboxylic acids that are associated with the C = O and C – O bonds of the carboxyl group [12]. In addition carboxylate ions show strong stretching vibrations at 1400–1280 and 1650–1510 cm^{-1} related to the symmetric and antisymmetric modes respectively [13]. The carboxylate ion is the position for

carboxylic acids coordination which is categorized as monodentate; chelating bidentate; and bridging bidentate depending on the separation of the carboxylate stretching bands [12, 14].

The stacked spectra (Fig. 1) are dominated by broad and intense absorptions at 1568 cm^{-1} and 1452 cm^{-1} corresponding to the carboxylate ions. The difference between these two band ($\Delta\bar{\nu}$ = $\bar{\nu}_{asym}$ - $\bar{\nu}_{sym}$ =1568 – 1452 = 116 cm^{-1}) designates chelating modes of coordination between the acid and the Zn atoms. The absence of the 1718 cm^{-1} carbonyl band of malonic acid is an indication of its binding to the surface of the nanoparticles. The Zn – O at 449 cm^{-1} bond, supports the chelating of the acid to the Zn atoms. Similarly, zinc succinate FTIR spectrum exhibits ($\Delta\bar{\nu}$ = $\bar{\nu}_{asym}$ - $\bar{\nu}_{sym}$ =1554 – 1417 = 137cm^{-1}) difference that corresponds to binding chelating mode. The band at 436 cm^{-1} confirms the attachment of Zn atoms to the acid. Likewise, zinc tartrate FTIR spectrum shows ($\Delta\bar{\nu}$ = $\bar{\nu}_{asym}$ - $\bar{\nu}_{sym}$ =1433 – 1363 = 70 cm^{-1}) difference that can be assigned to bridging binding mode. The band at 491 cm^{-1}, confirms the binding of Zn atoms to the acid. From the previous discussion, the chelation or coordination mode of carboxylate groups through their O atoms with Zn ions reveals asymmetric and symmetric stretching frequencies difference less than the ionic value ($\Delta\nu$ = 164 cm^{-1}) assigned to the acetate ion [12]. This indicates that the complexation is achieved through the carboxylate [15]and the IR data imply that the carboxylate group to the metal bonding is unidentate or pseudo-bridging [16].
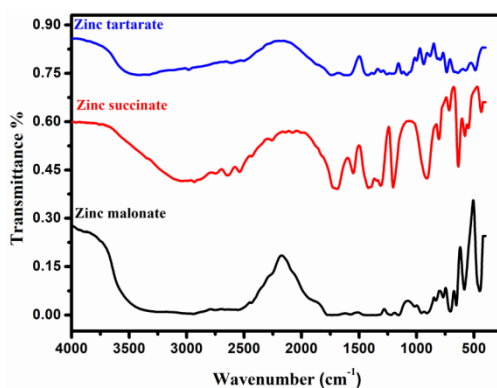

Fig. 1. FTIR spectra of the caroxylic acids zinc complexes.

The FTIR spectra of ZnO obtained after calcinations using the different carboxylic acids were studied at the 4000 – 400 cm^{-1}wavenumber range and the plots are displayed in (Fig. 2 a and b).The broad absorption bands at ≈ 3440, and 1100 cm^{-1} can be ascribed to the normal polymeric O-H stretching vibration of H$_2$O, in ZnO moiety [17]. The absorption band between 2300 and 2400 cm^{-1}indicates the absorption of atmospheric CO$_2$ molecule[18]. The chelating of the acid to the ZnO nanoparticles is supported by the Zn – O at 439 cm^{-1} [19].
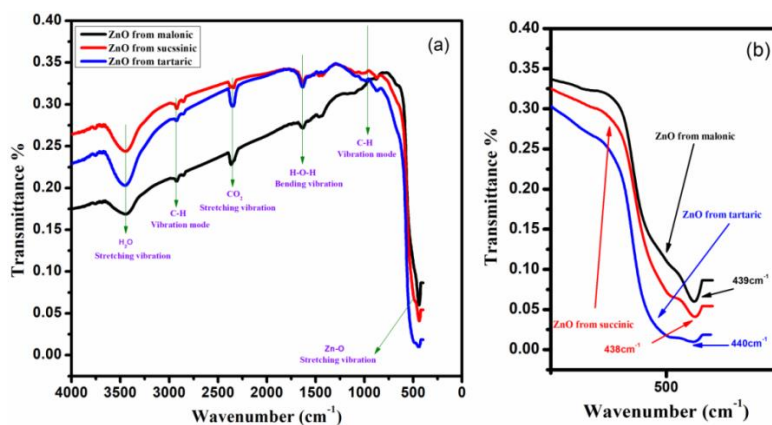

Fig. 2. FTIR spectra of the ZnO nanoparticles obtained from the carboxylic acids zinc complexes.

3.2. XRD analysis of ZnO nanopraticles

Fig. 3 illustrates the XRD graphs of ZnO nanoparticles prepared utilizing the different dicarboxylic acids. The entire images exhibitthe characteristic wurtzite (hexagonal phase)structure of ZnO. Wholeof the XRD peaks are in compliance with the (JCPDS) card No. 36-1451 [20]. All investigatedspecimenshave strong XRD linesmatchingwith the(1 0 1) plane.In addition, the diffraction peaks are narrow with higher intensityindicating good crystallite structure entities. Moreover, the (101) diffraction peaks broadening (Fig. 3b)reveals the nano-sizes of the fabricatedZnO nanoparticles (Table.1) as previously reported [21]. The average crystallite sizes (D) of the ZnO nanoparticleswere computedusing Debye Scherrer expression [22]:

$$D = \frac{0.90\lambda}{\beta\cos\theta}$$

(1)

where λ 1.5406 A^o is the Cu Kα line, Θ is the Braggs' XRD diffraction angle and β is the full width at half maximum(FWHM) in radians.The lattice parameters (a and c) for ZnO nanoparticles were calculated using equation (2). The plane d-spacing (d) is associated with the lattice parameters a, c and the Miller indices (h, k, l)and is calculated via the theoretical (3) and Braggs' equations (4) as well [23-25]:

$$a = \frac{\lambda}{\sqrt{3}\sin\theta_{100}} \text{ and } c = \frac{\lambda}{\sin\theta_{002}}$$

(2)

$$\frac{1}{d^2} = \frac{4}{3}\left[\frac{h^2+hk+k^2}{a^2}\right] + \frac{l^2}{c^2}$$

(3)

$$d = \frac{\lambda}{2\sin\theta}$$

(4)

where Θ_{100} and $\Theta_{002}$are the diffraction peaks angles of the (100) and (002) planes respectively. The values of the lattice parameters (a and c) (Table 1) are almost identical to those reported in the (JCPDS) card for ZnO[26].The d-spacing values obtained from the theoretical (3) and Braggs' law (4) equations, are approximately equal (Table 1).

The Zn–O bond length in the ZnO nanoparticles was calculated using equation (5)

$$\mathbf{L} = \sqrt{\left[\left(\frac{a^2}{3}\right) + (0.5-\mu)^2 . c^2\right]}$$

(5)

Where (μ) is the positional parameter in the wurtzite structure that indicate the extent of atom displacement relative to the next along the c axis, as expressed by equation (6):

$$\mu = \frac{a^2}{3c^2} + 0.25$$

(6)

The calculated ZnO bond lengths (Table.1) are in excellent agreement with the 1.9767A°reported in literature [27, 28].
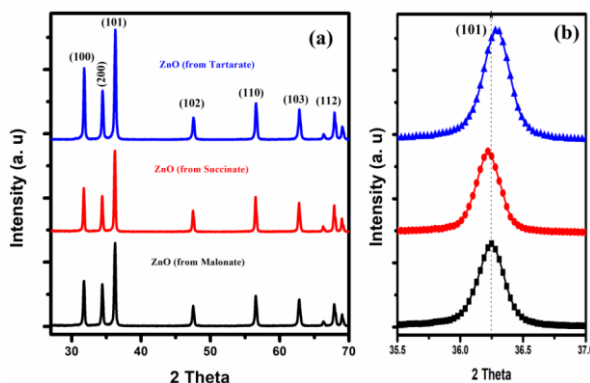
Fig. 3. XRD patterns of ZnO decomposed from (a) Zinc malonate (b) Zinc succinate and (c) Zinc tartrate.

Table 1. Lattice parameters of ZnO nanoparticles from XRD data.

Sample	D	Lattice strain	a	c	c/a	d*-spacing	d**-spacing	μ	$Zn - O$ (A^o)
ZnO_{Tart}	40.23	0.0027	3.2466	5.1952	1.6001	2.474	2.4737	0.3802	1.9751
ZnO_{Succ}	42.04	0.0025	3.2467	5.2098	1.6040	2.478	2.4748	0.3795	1.9768
ZnO_{Maln}	40.98	0.0027	3.2467	5.2099	1.6047	2.476	2.4744	0.3796	1.9768

* From XRD graph, ** Calculated

3.3. Williamson–Hall (W–H) methods for estimation of microstrain (ε) and crystallite size (D)

3.3.1. Uniform deformation model (UDM)

According to Williamson–Hall perspective[29], strain and crystallite size highly influence diffraction lines broadening (equation 7) [24, 30]. One of Williamson–Hall formulae is the Uniform Deformation Model (UDM). In UDM, it is presumed that crystals are isotropic[31]and as a result their properties are invariant with the direction measurements are carried out.

$$\beta_{hkl} \cos \theta_{hkl} = \frac{k\lambda}{D} + 4\varepsilon \sin \theta_{hkl} \tag{7}$$

Plotting $\beta_{hkl}.\cos\Theta_{hkl}$against4 $\sin\Theta_{hkl}$ gives a linear graph[31],where the crystallite size (*D*) and the microstrain (ε) can be sequentially obtained from the intercept and slope(Fig. 4).The obtained parameters are recorded in Table (2).
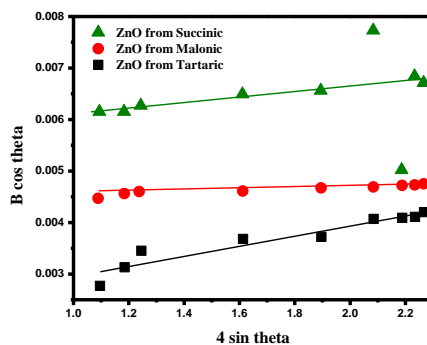

Fig. 4. UDM graphs for the ZnO samples annealed at (a) 275 ^{0}C,(b)375 ^{0}C, (c) 475 ^{0}C, and (d)600^{0}C.

3.3.2. Uniform stress deformation model (USDM)

In several instances, the isotropy and homogeneity supposition is unsatisfied and a better and more rational anisotropic model is hence considered. Thus, Williamson– Hall equation is remodeled by incorporating an isotropicity parameter of strain(ε)[32]. In (USDM), Hooke's law delineates the strain and sets a direct relationship between the stress (σ), anisotropic microstrain (ε) and Young's modulus (Y_{hkl})as set by $\sigma = \varepsilon Y_{hkl}$. A value of 127GPa is assigned to the (Y_{hkl}) of the hexagonal ZnO nanoparticles[24].Hence, the Williamson–Hall expression is rephrased to equation (8):

$$\beta_{hkl} \cos\theta_{hkl} = \frac{k\lambda}{D} + \frac{4\sigma \sin\theta_{hkl}}{Y_{hkl}} \tag{8}$$

Plotting $\beta_{hkl} . \cos\Theta_{hkl}$ versus $\frac{4\sin\theta_{hkl}}{Y_{hkl}}$ produces straight line from which the σ and $D$are

the slope and intercept respectively, while ε can be calculated applying Young's modulus, Y_{hkl}, of ZnO nanoparticles hexagon. Fig.(5) illustrates the USDM for the samples and the values obtained are tabulated (Table 2).
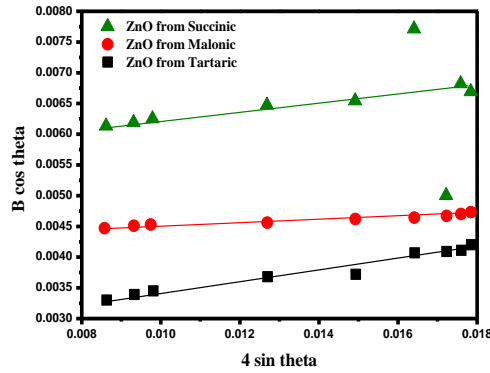

Fig. 5.USDM for the four ZnO samples (a) 275 ^{0}C, (b) 375^{0}C, (c) 475^{0}C and (d) 600^{0}C.

3.3.3. Uniform deformation energy density model (UDEDM)

One more form of Williamson– Hall approach termed the Uniform Deformation Energy Density Model (UDEDM) is applied to find the crystal's energy density (u_{ed}).For elastic systems that obey Hooke's law, u_{ed} and strain are related by the formula $u_{ed} = (\varepsilon^2 Y_{hkl})/2$[24].Equation (9) provides the UDEDM equation:

$$\beta_{hkl} \cos\theta_{hkl} = \frac{k\lambda}{D} + \left(4\sin\theta_{hkl}(\frac{2\mu_{ed}}{Y_{hkl}})^{0.5} \right) \tag{9}$$

where
$$\left(\frac{2}{Y_{hkl}} \right)^{0.5} = 0.1255$$

From $\beta_{hkl.} cos\Theta_{hkl}$ versus $4\sin\theta_{hkl}\left(\frac{2}{Y_{hkl}} \right)^{0.5}$ plot, we can get the anisotropic energy density

(μ_{ed}) from the slope, stress σ, microstrain ε are calculated from (μ_{ed}) and, while the crystallite size (D) is estimated from intercept[24].Fig.(6) displays the USDM for the samples and the results obtained are listed in Table (2)
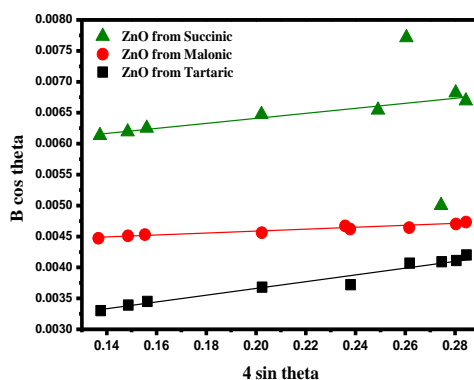
Fig. 6. UDEDM for the ZnO samples at (a) 275 ^0C, (b) 375 ^0C, (c) 475 ^0C and (d) 600 ^0C.

The mean crystallite size values applying the UDM, UDSM, and UDEDM models are virtually identical, indicating that the insertion of strain in the different formulae of W–H method has insignificant impact on the average (*D*) value. Nevertheless, the average crystallite sizes calculated from Scherer and W–H equations show little disparity that can be attributed to dissimilarity of particle size distribution averaging [33].

Table2. Particle size and crystallite size calculated using Scherrer and Williamson- Hall models.

Sample	Scherrer D (nm)	Williamson- Hall method								
		UDM		USDM			UDEDM			
		D (nm)	ε x 10^{-4}	D (nm)	ε x 10^{-4}	σ (MPa)	D (nm)	ε x 10^{-4}	σ(MPa)	u_{ed}(KJm^{-3})
ZnO $_{tar}$	43.40	70.38	9.82	54.80	7.12	90.44	54.8	5.67	72.01	2.041
ZnO $_{Mal}$	42.80	44.58	1.82	55.58	1.83	23.20	45.2	1.52	19.30	0.147
ZnO $_{suc}$	46.20	50.60	3.21	49.88	3.03	38.47	50.24	2.38	30.23	0.360

3.4. Morphology of ZnO nanoparticles

The shape and size of the nanoparticles was inspected by (SEM) as displayed in Fig. 7. It is known that XRD provides the crystallite and not particle size. Thus the values of grain sizes estimated using SEM images is obviously larger than those given by XRD data. Alternatively, we can indicate that the SEM photos point out the polycrystalline size of particles. The observed larger nanoparticles can be attributed to the affinity to agglomerate due to the high surface energies of particles with spherical morphology [34]. The SEM images show that all of the particles obtained are acquiring a nearly spherical shape. The average diameter of the spheres decreases continuously in the order: succinic acid (168 nm) > malonic acid (127 nm) > tartaric acid (85 nm). This finding indicates the effect of carboxylic acid on the particles size as has been reported by Monfared *et al*. who prepared different size (Fe$_3$O$_4$-NPs) using different carboxylic acids [7]. At elevated temperature agglomeration and other thermal effects like Ostwald ripening lead to the preferential formation of the energetically favored larger particles rather than the ones of smaller sizes[35]. This can be accredited to the reality that particles' surface molecules are energetically less stable compared to those ordered and packed into the interior. Thus, the structure endeavors to minimize its energy and consequently molecules at surfaces of smaller particle will diffuse and aggregate on the larger particle surface. Hence, the smaller particles will shrivel and the larger particles will develop in size [35].

Fig. 7.SEM images of ZnO decomposed from (a) Zinc malonate (b) Zinc succinate and (c) Zinctartrate.

3.5. Thermogravimetric analysis

The thermal decomposition of zinc precursors of the three samples as examined by TGA and derivative weight / temperature analysis, is displayed in Fig. 8 (a – c). In all graphs a first stage with a mass loss of about 30 %is observable when the temperature attained ≈ 150°C followed with an increased weight loss of 60 % at 200°C. This mass loss may be attributed to the removal of hydroxyl groups and moisture[36] as supported with two sharp endothermic peaks at these temperature values. Another apparent loss of 20 %and an endothermic peak appear at ≈ 400°C which may have resulted from the decomposition of the carboxylate ions (accompanied by the evolution of large amount of gases such as CO, CO_2, water and vapor) and other organic functional groups attached to the ZnO moiety[37]. The TGA graph of zinc tartarate (Fig. 8 c) shows two decomposition step of ≈ 40 % each at 250 and 400°C. This dissimilar behavior may be attributed to the two OH groups attached to tartaric acid molecule. The steady weight beyond 400°C signifies the stability and formation of the target ZnO nanoparticles. Moreover, this finding indicates that 400°C is appropriate annealing temperature for the prepared sample.

Fig. 8. TGA and derivative weight / Temperature of ZnO decomposed from
(a) Zinc malonate (b) Zinc succinate and (c) Zinc tartarate.

3.6. Photoluminescence study of ZnO nanoparticles

ZnO visible emission was justified by two accepted mechanisms: the recombination of shallow trapped electrons with deep trap holes [38] or the recombination of electrons trapped in singly charged oxygen vacancy (V_{O_+}) with the photo-generated holes in the valence band [39]. Fig. 9 demonstrates the evolution of the PL spectra of ZnO nanoparticles synthesized with the different carboxylic acids. All spectra show a blue emission at 495[40]and green emission at 520 nm. The green emission may be featured to electrons transitions from surface states deep donor level oxygen vacancies to valence band[41].The blue emission may be ascribed to electronic transition from donor energy level of zinc interstitial to acceptor energy level of zinc vacancies[42]. Although Xiong *et al*. [43] reported a monotonous increase in exciton intensities with the crystallite size, we observed a contradictory effect as the intensity decreased in case of Zn_{sccu} which has the largest size (Table 1). Our finding agrees with that of Yadav *et al*. [44] who concluded that the intensity of green luminescence was enhanced by the decrease in ZnO particle size and attributed that to the increased surface to volume ratio.
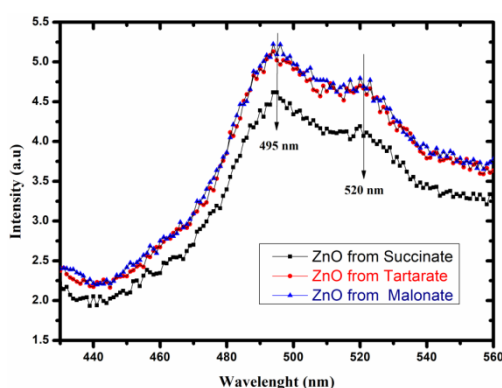

*Fig. 9. PL spectra of ZnO nanoparticles synthesized from
the different carboxylic acids.*

4. Conclusion

A facile approach for the fabrication of zinc oxide nanoparticles is reported in this study. The ingredients employed for that were aqueous solutions of zinc nitrate and dicarboxylic acids. The obtained target nanostructures was confirmed by XRD, William Hall models, SEM and FTIR. The optical properties of the as prepared ZnO nanoparticles reflected two emission peaks in the blue and green regions of the spectrum. Finally, it can be concluded that a simple method for zinc oxide nanoparticles synthesis without adding harmful chemicals was achieved through this work.

Acknowledgement

References

[1] M.Vafaee, M.S. Ghamsari, Materials Letters **61**(14-15), 3265 (2007).
[2] K.C.Pradel, et al., Nano Letters **14**(12), 6897 (2014).
[3]K.Ellmer, Nature Photonics **6**(12), 809 (2012).
[4] J.S.Park, et al., Thin Solid Films **520**(6), 1679 (2012).
[5] M.Vafaee, M.S. Ghamsari, S. Radiman, Journal of Luminescence **131**(1), 155 (2011).
[6] G.Du, et al., Journal of Materials Science**45**(6), 1464 (2010).

[7] H.Hosseini-Monfared, F. Parchegani, S. Alavi, Journal of Colloid and Interface Science **437**, 1 (2015).

[8] R.L.Fomekong, et al., Journal of Solid State Chemistry **230**, 381 (2015).

[9]D.Gingasu, et al., Ceramics International **40**(1), 2267 (2014).

[10] R.L.Fomekong, et al., Sensors and Actuators B: Chemical **231**, 520 (2016).

[11]M. Estruga, C. Domingo, J.A. Ayllón, Journal of Materials Chemistry **21**(12), 4408 (2011).

[12] G.Gliemann, K. Nakamoto, John Wiley and Sons, New York, Chichester, Brisbane, Toronto 1978. 3. Aufl., XV, 448 Seiten mit 109 Abbildungen und 95 Tabellen,**15**. Berichte der Bunsengesellschaft für physikalische Chemie **82**(11), 1263 (1978).

[13]J.Jia, et al., Journal of Colloid and Interface Science **379**(1), 1 (2012).

[14] Y.T.Tao, Journal of the American Chemical Society **115**(10), 4350 (1993).

[15] W.Beck, K. Nakamoto,4. Auflage, John Wiley & Sons, New York, Chichester, Brisbane, Toronto, Singapore 1986. 484 Seiten, Berichte der Bunsengesellschaft für physikalische Chemie **92**(4), 561 (1988).

[16] G.Deacon, R. Phillips, Coordination Chemistry Reviews **33**(3), 227 (1980).

[17] M.Ashokkumar, S. Muthukumaran, Superlattices and Microstructures **69,** 53 (2014).

[18] M.Arshad, et al., Journal of Alloys and Compounds **509**(33), 8378 (2011).

[19] K.D.Dobson, A.J. McQuillan, Spectrochimica Acta Part A: Molecular and Biomolecular Spectroscopy **55**(7-8), 1395 (1999).

[20] S.J. Chipera, D.L. Bish, Advances in Materials Physics and Chemistry **3**(01), 47 (2013).

[21] N.Singh, 2013.

[22] C.S.Barrett, 1943: McGraw-Hill Book Company, Inc.; New York.

[23] U.Seetawan, et al., Materials Sciences and Applications **2**(09), 1302 (2011).

[24] T. Pandiyarajan, B. Karthikeyan, Journal of Nanoparticle Research **14**(1), 647 (2012).

[25] U.Pal, et al. Optical Materials **29**(1), 65 (2006).

[26] F.H.Chung, Journal of Applied Crystallography **7**(6), 526 (1974).

[27] A.Modwi, et al., Journal of Ovonic Research **12**(2),(2016).

[28]K.Taha, M. M'hamed, H. Idriss, J. Ovon. Res.**11**(6), 271 (2015).

[29] A.K.Zak, et al., Ceramics International **42**(12), 13605 (2016).

[30] P.Bindu, S. Thomas, Journal of Theoretical and Applied Physics **8**(4), 123 (2014).

[31] T. Ungár, Journal of Materials Science **42**(5), 1584 (2007).

[32] S.Brandstetter, et al., Acta Materialia **56**(2), 165 (2008).

[33] A.K.Zak, et al., Solid State Sciences**13**(1), 251 (2011).

[34] M.Przybyszewska, et al., Journal of Chromatography A **1216**(27), 5284 (2009).

[35] M.Gondal, et al., Applied Surface Science **256**(1), 298 (2009).

[36]A.Moezzi, et al., Journal of Nanoparticle Research **16**(4), 2344 (2014).

[37] J.Shah, R.K. Kotnala, Journal of Physics and Chemistry of Solids **108**, 15 (2017).

[38] A.Van Dijken, et al., Journal of Luminescence **87**, 454 (2000).

[39] K.Vanheusden, et al., Journal of Applied Physics **79**(10), 7983 (1996).

[40] M.Popa, et al., Journal of Alloys and Compounds **574**, 255 (2013).

[41] Y.Gong, et al., Nanoscale Research Letters **2**(6), 297 (2007).

[42] B.Efafi, M.M. Ara, S. Mousavi, Journal of Luminescence **178**, 384 (2016).

[43]G.Xiong, U. Pal, J.G. Serrano, Journal of Applied Physics **101**(2), 024317 (2007).

[44] H.K.Yadav, et al., Journal of Materials Research **22**(9), 2404 (2007).